The Fatigue Response and Fracture Behavior of a Spray Atomized and Deposited Aluminum-Silicon Alloy

T.S. Srivatsan, S. Anand, Y. Wu, and E.J. Lavernia

In this article the results of a recent study designed to improve our understanding of the cyclic fatigue and fracture characteristics of a spray atomized and deposited hypereutectic aluminum-silicon alloy are presented. Specimens of the alloy were cyclically deformed to failure at ambient temperature under fully reversed total strain amplitude controlled tension-compression loading. The alloy exhibited low cyclic plasticity and fatigue life under total strain amplitude controlled deformation. Cyclic stress amplitude controlled high-cycle fatigue characteristics were established at an elevated temperature (150 °C). The cyclic stress response, high-cycle fatigue life and fracture characteristics of the alloy are compared with a conventional ingot metallurgy processed counterpart and discussed in light of intrinsic microstructural features, nature and magnitude of stress, and ductility of the material.

Keywords aluminum alloys, cyclic fatigue, deformation, fracture, microstructure

1. Introduction

Major strides in technological advancements coupled with the sustained requirement for high-performance materials, which besides offering light weight and extended high-temperature durability can provide adequate ductility and good fatigue and damage tolerance characteristics, have in the most recent decade engineered considerable scientific interest in aluminum-silicon alloys with hypereutectic compositions. The low coefficient of thermal expansion (CTE) coupled with excellent wear-resistance characteristics, derived from the presence of a high volume fraction of the silicon phase, have provided the additional impetus for considering the family of hypereutectic aluminum-silicon alloys as potentially viable candidates for a spectrum of demanding applications in the aerospace, automotive, and electrical industries (Ref 1-3). Recent efforts to engineer enhanced physical and mechanical properties have focused on using innovative processing techniques and modifications to alloy composition as affordable and alternative approaches for improving the strength, ductility, fracture toughness, fatigue resistance, and fracture-related properties of these alloys (Ref 4-6).

The extensive use of conventional ingot metallurgy (I/M) processing as a viable and economically affordable technique was hampered by the range of allowable alloy compositions. This can be attributed to the presence of coarse primary silicon along with other eutectic phases. These phases result as a direct consequence of the low solidification rate that is typical of (I/M) processing. The presence and distribution of coarse particles of silicon in an aluminum alloy matrix is largely responsible for the inferior ductility, inadequate fracture resistance, and limited workability (fabricability) of the family of I/M-processed hypereutectic aluminum-silicon alloys (Ref 4). To obviate many of the problems arising from conventional I/M processing, rapid solidification processing (RSP), such as melt spinning (Ref 7), atomization (Ref 2, 3), and spray deposition (Ref 8) emerged as attractive and potentially viable alternatives. The noteworthy advantage in the use of RS processing is an achievement of significant modifications in the size, morphology, and distribution of the primary silicon phase in the alloy matrix, relative to that present in a conventionally processed counterpart.

The primary objective for this study was to provide an insight into the cyclic fatigue and fracture behavior of a spray atomized and deposited hypereutectic aluminum-silicon alloy. The cyclic fatigue response and fracture characteristics of the spray-processed alloy is compared with a conventional I/M processed counterpart of identical chemical composition.

T.S. Srivatsan and **S. Anand,** Department of Mechanical Engineering, The University of Akron, Akron, Ohio 44325-3903, USA; and **Y. Wu** and **E.J. Lavernia,** Department of Chemical Engineering and Materials Science, University of California, Irvine, CA 92697, USA.

2. Material and Processing

High-deposition-rate spray deposition processing is an attractive technique that offers an opportunity to transform a molten alloy into a high-quality consolidated product. In this last decade, the technique has been successfully used to synthesize a spectrum of engineering alloys and their composite counterparts (Ref 9-18). The technique of spray atomization and deposition processing is essentially a two-step process route that involves (Ref 13-15, 19-21):

1. Atomization of a stream of molten metal, using an inert gas, producing a spray of micron-sized liquid droplets
2. Deposition of the droplets, a mixture of solid and semi-solid (partially solidified), on a substrate surface

The micron-sized droplets are relatively free from segregation, are low in oxygen content, and exhibit enhanced hot workability. The droplets collect as a coherent preform, the microstructure of which is governed by the solidification conditions of the droplets during impact with the substrate. Details of the

technique and microstructural characteristics of spray atomized and deposited materials are discussed elsewhere (Ref 17-21).

The starting material used in this study was commercial-quality cast aluminum alloy A390 (provided by Reynolds Metals Company, Richmond, VA) in the form of ingot bars. The nominal chemical composition (in wt%) of the as-received material is Al-17Si-4.5Cu-0.6Mg. Samples of the rapidly solidified (RS) hypereutectic alloy, of identical composition to the cast I/M counterpart A390, were prepared by utilizing a spray atomization and deposition approach, henceforth referred to in this article as spray processed. The synthesis involves the following procedure:

1. The as-received A390 alloy was superheated to a temperature of 1073 K in a graphite crucible in an environment of nitrogen (N_2) gas at 1 atm pressure. To avoid oxidation of the hypereutectic aluminum-silicon alloy during spray deposition processing, the experiments were conducted inside an environmental chamber that was evacuated down to a pressure of 200 Pa and backfilled with nitrogen.
2. The superheated alloy was delivered to an atomizer through a ceramic delivery tube, where it was disintegrated into a fine dispersion of micron-sized droplets using nitrogen gas and at a atomization pressure of 3.1 MPa.
3. Following atomization, the partially solidified droplets were collected on a hydraulically controlled, water-cooled, rotating copper substrate, positioned at a distance of 46 cm from the atomizer nozzle. The droplets collect as a coherent preform.

Details of the apparatus and the processing parameters used can be found elsewhere (Ref 13).

The as-spray-deposited material was sectioned into billets 2.54 cm in diameter by 8 cm length. The billets were hot extruded at 773 K using an extrusion ratio of 16 to 1. The purpose of extruding at an elevated temperature was to close the micrometer-sized pores typical of spray atomized and spray deposited materials (Ref 8, 22). The extruded bar was allowed to cool in ambient air. Henceforth in this article, the spray deposited and thermomechanically processed wrought alloy will be designated as AS17.

3. Experimental Techniques

3.1 *Initial Microstructure*

The initial microstructure of the spray deposited plus extruded alloy and the conventional I/M processed (as-sand-cast) counterpart was characterized by optical microscopy after specimen preparation by standard metallography and polishing techniques. The samples were etched with Keller's reagent and examined in an optical microscope and photographed using a standard bright-field illumination technique to reveal: the grain boundaries, second-phase morphology and distribution, and overall grain morphology. The primary and other secondary phases present in the microstructure were identified using transmission electron microscopy (TEM), selected area diffraction (SAD), and x-ray diffraction (XRD). The TEM studies were conducted using a Phillips CM20 transmission electron microscope operated at an accelerating voltage of 200 keV.

3.2 *Tensile and Fatigue Testing*

Tensile and fatigue test samples, conforming to specifications in ASTM E-8-93 (Ref 22), were precision machined from both the spray processed (AS17) and I/M (A390) alloys. The test specimens were smooth and cylindrical in the gage section. The machined surfaces of the test specimens were mechanically ground and finish polished using progressively finer grades of SiC impregnated emery paper to remove all circumferential scratches and surface-machining marks. Total strain amplitude-controlled and stress amplitude-controlled fatigue tests were performed on a fully automated closed-loop servo-hydraulic test machine equipped with a 100 kN load cell. Fully reversed, push-pull, tension-compression total strain amplitude ($R_\varepsilon = \varepsilon_{min}/\varepsilon_{max} = -1$) controlled low-cycle fatigue tests were conducted in controlled laboratory air environment (relative humidity of 55%) at ambient temperature (30 °C). The total strain amplitude-controlled tests were performed at a constant strain rate of 1×10^{-3}/s. The strain function exhibited a triangular waveform and the mean strain was zero. The test was initiated in tension. The axial strain was monitored with a 12.7 mm clip-on extensometer fixed to the gage section of the test specimen using steel springs. The stress and strain measurements, parallel to the load line, were recorded on a PC-based data acquisition system. In view of the limited cyclic ductility, cyclic strain resistance, and resultant low-cycle fatigue life of the alloy at ambient temperature, the stress amplitude-controlled high-cycle fatigue tests were conducted in the laboratory air environment at an elevated temperature of 150 °C. The elevated temperature chosen corresponded to the maximum temperature limit of the environmental chamber unit. The elevated-temperature tests were conducted using an Instron Environmental Chamber (Model 3111). The temperature was controlled with the aid of a temperature controller in conjunction with a thermocouple. The thermocouple was fixed onto the surface of the specimen. Maximum temperature variation was well within 2 °C of the set-point temperature (150 °C) over the entire duration of the test. Ambient temperature varied from 30 to 33 °C during any given test. Before each test, the specimen was maintained at the test temperature for 30 min to achieve stability with the environment. The tests were conducted at a constant cyclic frequency of 1 Hz and at a stress ratio ($R = \sigma_{min}/\sigma_{max}$) of 0.1. The number of cycles to cause complete failure or separation is taken as fatigue life (N_f).

3.3 *Failure-Damage Analysis*

Fracture surfaces of the deformed and failed test samples were examined in a scanning electron microscope (SEM) to determine the macroscopic fracture mode and to characterize the fine-scale topography and microscopic mechanisms governing fracture. The distinction between the macroscopic mode and microscopic fracture mechanism is based on the magnification level at which the observations are made. The macroscopic mode refers to the nature of failure, while the microscopic mechanism relates to the local failure processes (microvoid formation, coalescence, and nature of cracking). Samples for

SEM observation were obtained from the failed fatigue specimens by sectioning parallel to the fracture surface.

4. Results and Discussion

4.1 *Microstructure*

The optical micrographs of the conventional I/M processed (as-sand-cast, A390) and the spray deposition processed (AS17) counterpart are shown in Fig. 1 and 2. The microstructure of the conventionally processed A390 alloy, in the as-cast plus extruded condition, reveals the primary silicon particulates, of varying size, distributed randomly through the alloy matrix (Fig. 1a). The nonuniform size and distribution of the particulates resulted in particulate-rich and particulate-depleted regions (Fig. 1b). The particulates were aligned in the direction of extrusion. Besides the presence of blocklike silicon particulates, isolated pockets of a eutectic silicon phase, having a flakelike morphology with a large aspect ratio, was also evident (Fig. 1c). Transmission electron microscopy observations revealed secondary phases decorating the interdendritic

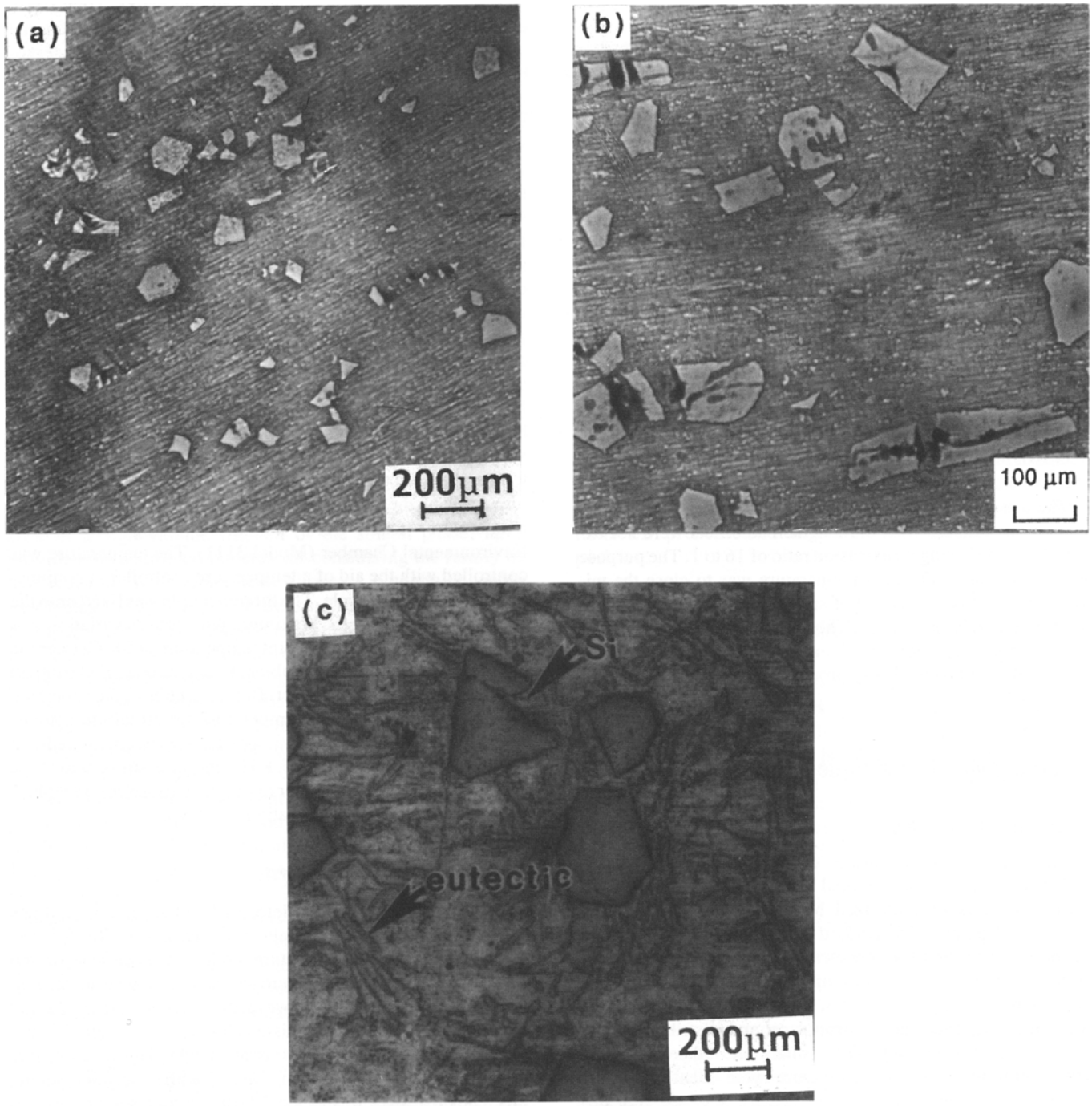

Fig. 1 Optical micrographs showing microstructure of the conventional I/M-processed (as-sand-cast) alloy A390

boundaries of the α-aluminum phase. In an earlier study, these phases were identified by electron diffraction to be the Al_2Cu and Al_xCu_yMg (Ref 18).

Optical microstructure of the spray deposition processed (AS17) alloy revealed a near-uniform distribution of dispersoids (Fig. 2a) and equiaxed-shaped grains (Fig. 2b). The presence of eutectic Al-Si phase and coarse primary silicon particulates in the conventionally I/M-processed counterpart was suppressed. The dispersoids present in the α-aluminum matrix exhibited a faceted particulate morphology. Factors contributing to the formation and presence of the particulatelike silicon phase in the spray deposited microstructure can be found elsewhere (Ref 6, 18). The presence of near-equiaxed-shaped grains (Fig. 2b) conforms well with results obtained by other investigators on both the reinforced and unreinforced spray deposited materials of various compositions (Ref 23-27). The two governing mechanisms that have been proposed to explain the formation of equiaxed grains in spray processed materials are:

- Equiaxed grain formation by the fragmentation of dendrite arms (Ref 19, 23, 26, 27).
- Equiaxed grain development by the progressive growth and eventual coalescence of the dendrite fragments during solid-state cooling (Ref 23).

The tensile properties of the two alloys are summarized in Table 1. The spray deposition processed material (AS17) had better strength (yield strength and ultimate tensile strength) than the conventional I/M (as-sand-cast: A390) counterpart. The improvement in strength was found to have little influence on tensile ductility. Mechanisms responsible for the improved strength of the spray processed material are discussed in detail elsewhere (Ref 6).

4.2 *Cyclic Fatigue Response*

The variation of stress response with fatigue cycles, for a test conducted at cyclic total strain amplitude ($\Delta\varepsilon_T/2$) of 0.7, is an important feature of the fully reversed, tension-compres-

Table 1 Tensile properties of the conventional I/M-processed and spray processed alloys

Alloy	Process	Temperature, °C	Young's modulus(a) GPa	Young's modulus(a) 10^6 psi	Yield strength MPa	Yield strength ksi	Ultimate tensile strength MPa	Ultimate tensile strength ksi	Elongation,s %	Reduction in area, %	True strain ln (A_0/A_f), %
A390	Sand cast and extruded	27	78	11.3	390	57	424	61	2.4	6.0	7.0
		150	70	10.2	283	42	287	42	0.8	2.0	3.0
AS17	Spray atomized and deposited	27	80	11.6	411	60	448	65	2.8	6.0	7.0
		150	80	11.6	343	50	355	52	2.44	5.0	7.0

(a) Tangency measurement based on extensometer trace

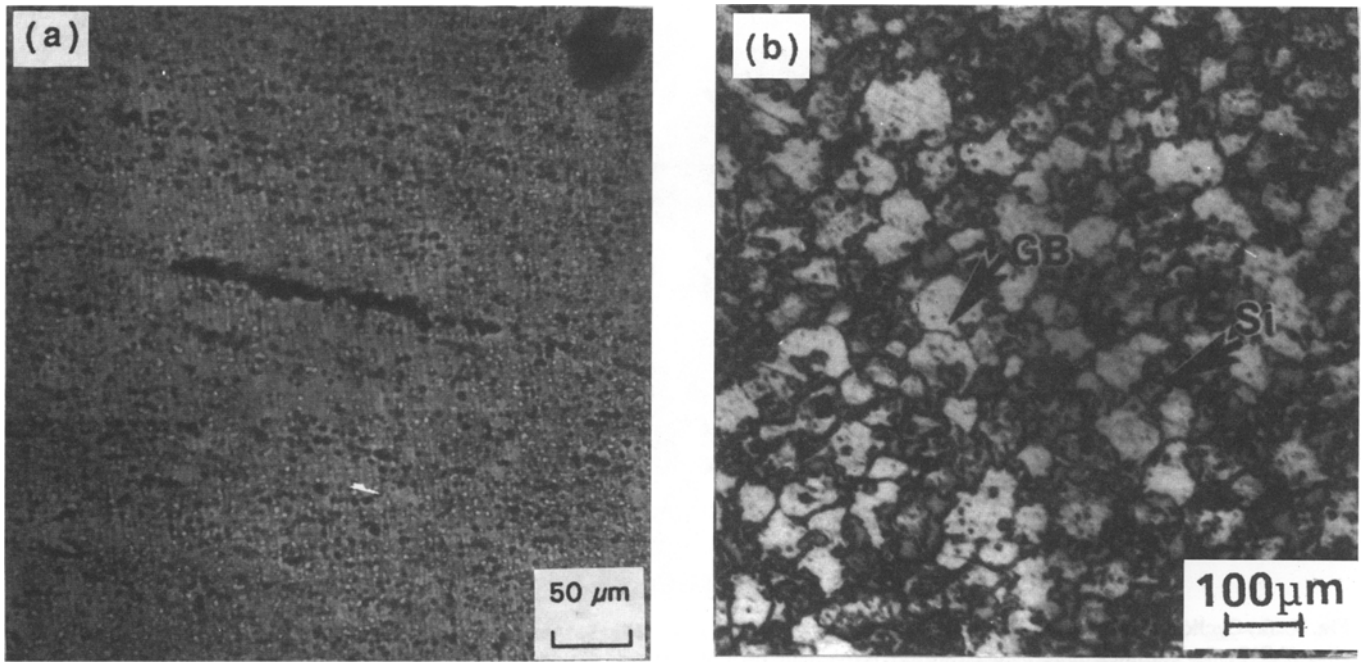

Fig. 2 Optical micrographs showing microstructure of the spray deposition processed (spray atomized and deposited plus extruded) alloy

sion, strain amplitude controlled fatigue tests. The stress amplitude ($\Delta\sigma/2$) versus cycles (N) curve was obtained by monitoring the stress range ($\Delta\sigma$) during total strain amplitude controlled fatigue (Fig. 3). The curve provides useful information pertaining to both the cyclic and overall mechanical stability of the microstructure during cyclic plastic deformation. The curve illustrates the path taken by the spray deposition processed material to its final flow stress level. At a constant total strain amplitude-control ($\Delta\varepsilon_T/2 = 0.70\%$), the cyclic plastic strain amplitude ($\Delta\varepsilon_p/2$) varied throughout the test reaching a maximum value at the minimum stress amplitude and a minimum value at the maximum stress amplitude. For purposes of reference the value at specimen half-life ($N_f/2$) is taken. At the total strain amplitude ($\Delta\varepsilon_T/2 = 0.70$) investigated, the spray atomized and deposited microstructure showed very little evidence of cyclic plasticity, although progressive softening occurred from the onset of fully reversed cyclic deformation. The variation of normalized stress (σ_N/σ_1) with fatigue cycles (N), where the cyclic stress amplitude at any cycle (σ_N) is normalized with respect to the cyclic stress amplitude of the first cycle (Fig. 3b), confirms the observation of progressive softening to failure. Normalized stress reveals the alloy undergoing rapid initial softening followed by gradual softening to failure. Variation of the cyclic tensile and compressive stresses, during fully reversed strain cycling, reveals the observed softening to occur as a result of a progressive decrease in both the tensile and compressive stresses from the onset of fully reversed cyclic deformation (Fig. 4). The observed decrease in stress is attributed to the initiation and presence of numerous microscopic and macroscopic cracks, and their progressive growth through the alloy microstructure and eventual coalescence, from the onset of fully reversed cyclic straining. Because of limited ambient temperature cyclic ductility and low-cycle fatigue life of the spray deposition processed microstructure, under conditions of fully reversed strain cycling, the total strain amplitude ($\Delta\varepsilon_T/2$) controlled cyclic fatigue test was restricted to one performed at 0.70%.

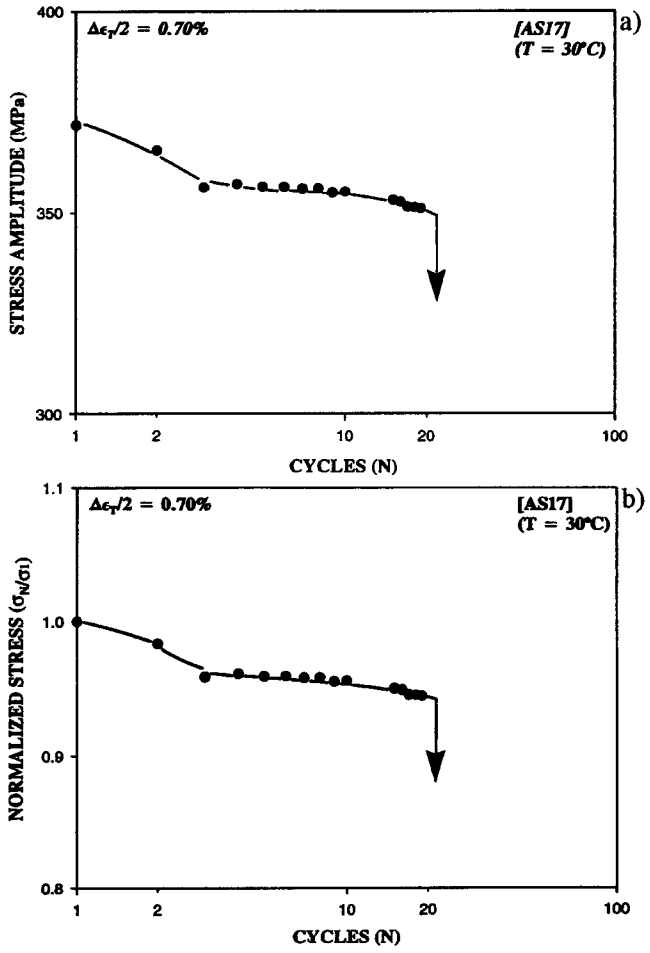

Fig. 3 (a) Cyclic stress response curve for the spray processed alloy (AS17). (b) Variation of normalized stress (σ_N/σ_1) with fatigue cycles (N) for the spray processed alloy AS17

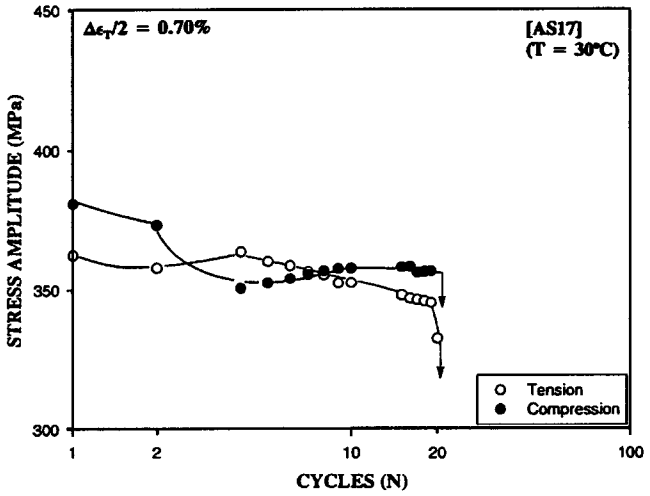

Fig. 4 Variation of the tensile and compressive stresses with cycles for the spray deposition processed aluminum-silicon alloy, under conditions of strain amplitude controlled fatigue deformation, at ambient temperature

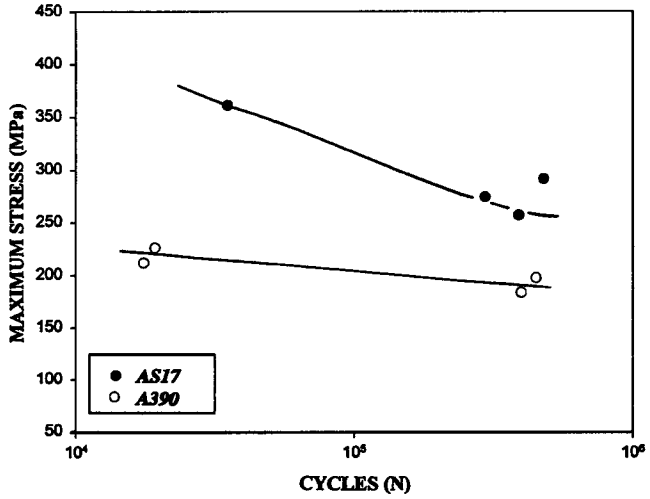

Fig. 5 A comparison of the variation of maximum stress (σ_{max}) with fatigue life (N_f) for the spray deposition processed (AS17) and the I/M (as-sand-cast: A390) alloys

The stress amplitude-controlled high-cycle fatigue test provides information pertinent to the existence of an endurance or fatigue limit. In the high-cycle, low-stress amplitude fatigue of the spray deposition processed aluminum-silicon alloy, the property changes are confined to occur at and around the vicinity of the fracture process zone at the crack tip, while the material in the far field remains relatively unaffected during fatigue cycling. The results of the axial stress amplitude-controlled tests are shown in Fig. 5, as the variation of maximum stress (σ_{max}) with cycles to failure (N_f). There is an absence of a well-defined fatigue limit or plateau in the stress-fatigue life curve as is typical for the family of ferrous-base alloys. The maximum stress-fatigue life curve exhibits the general trend shown by nonferrous metals and their composite counterparts. It is observed that the spray deposition processed alloy (AS17) can withstand higher cyclic stress than the conventional I/M-processed (as-sand-cast) counterpart (A390). At equivalent cyclic stress amplitudes the spray deposition processed material (AS17) reveals at least two to three orders improvement in high-cycle fatigue life ($N_f > 10^4$ cycles) over the conventional I/M processed counterpart.

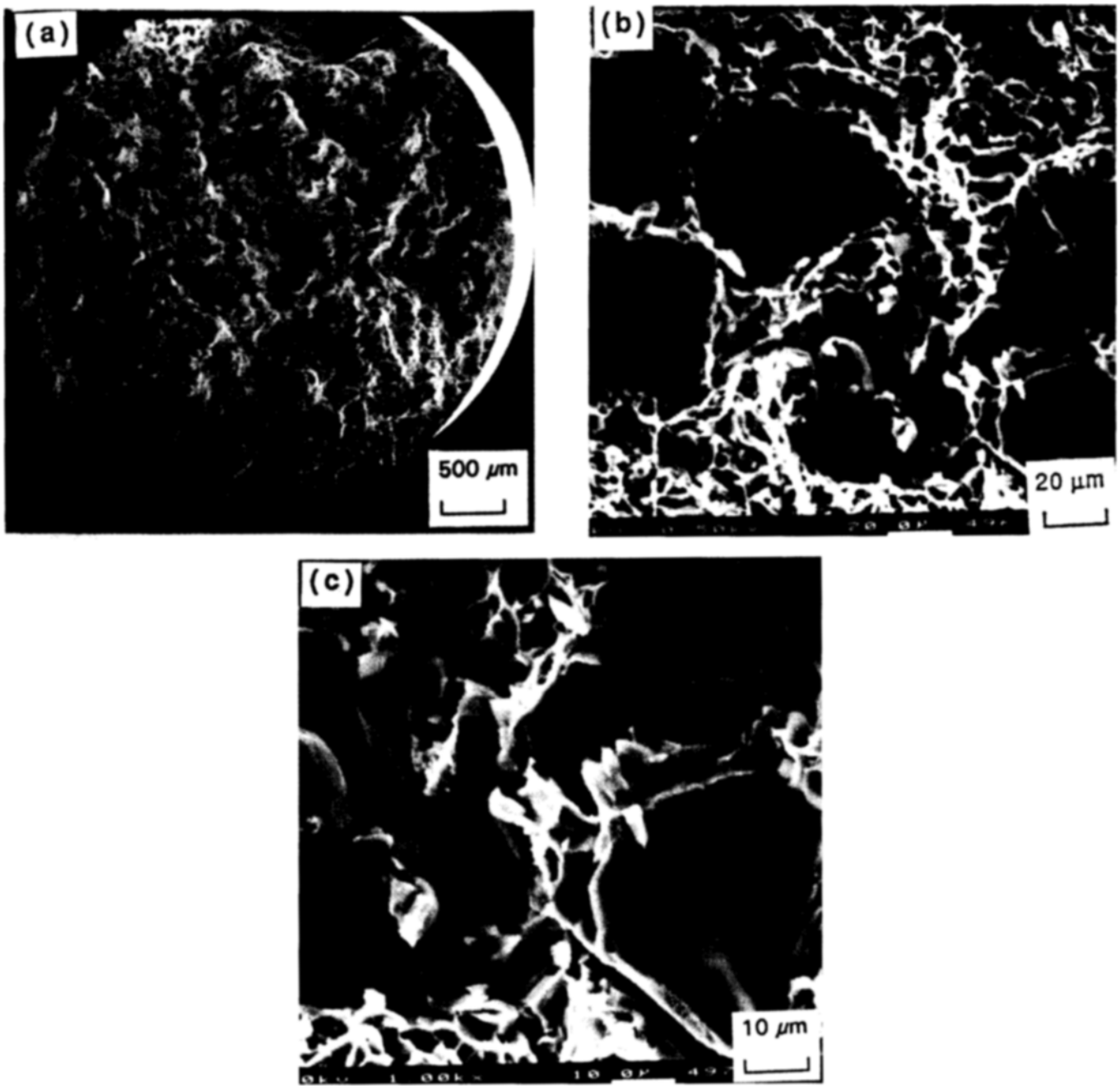

Fig. 6 Scanning electron micrographs of the high-cycle fatigue fracture surface of the I/M-processed (as-sand-cast) alloy (σ_{max} = 226 MPa, N_f = 19,261 cycles) showing (a) overall morphology showing random distribution of voids, (b) cracked particles, and (c) cracked particles and interface failure/decohesion

4.3 *Cyclic Fracture Behavior*

Examination of the stress amplitude controlled fatigue fracture surfaces of the spray deposition processed and conventional I/M processed alloys was done at:

- Low magnifications to identify the regions of microcrack initiation, stable microscopic crack growth, and final fracture
- Higher magnifications in the region of stable crack growth to identify the location and distribution of fine microscopic cracks and nature of microscopic crack growth and the region of overload to identify the fine-scale fracture features

Representative fracture features of the two alloys are shown in Fig. 6 to 9.

4.3.1 Conventionally Processed Alloy (A390)

High-cycle-fatigue (HCF) fracture surfaces of the alloy, deformed at a maximum cyclic stress of 226 MPa (N_f: 19,261 cycles), revealed fracture to occur on a plane that was essentially normal to the far-field stress axis. The fracture surfaces revealed a small region of fatigue and a large portion to be overload failure with little to no evidence of cyclic ductility. Low-magnification observations revealed cracked silicon par-

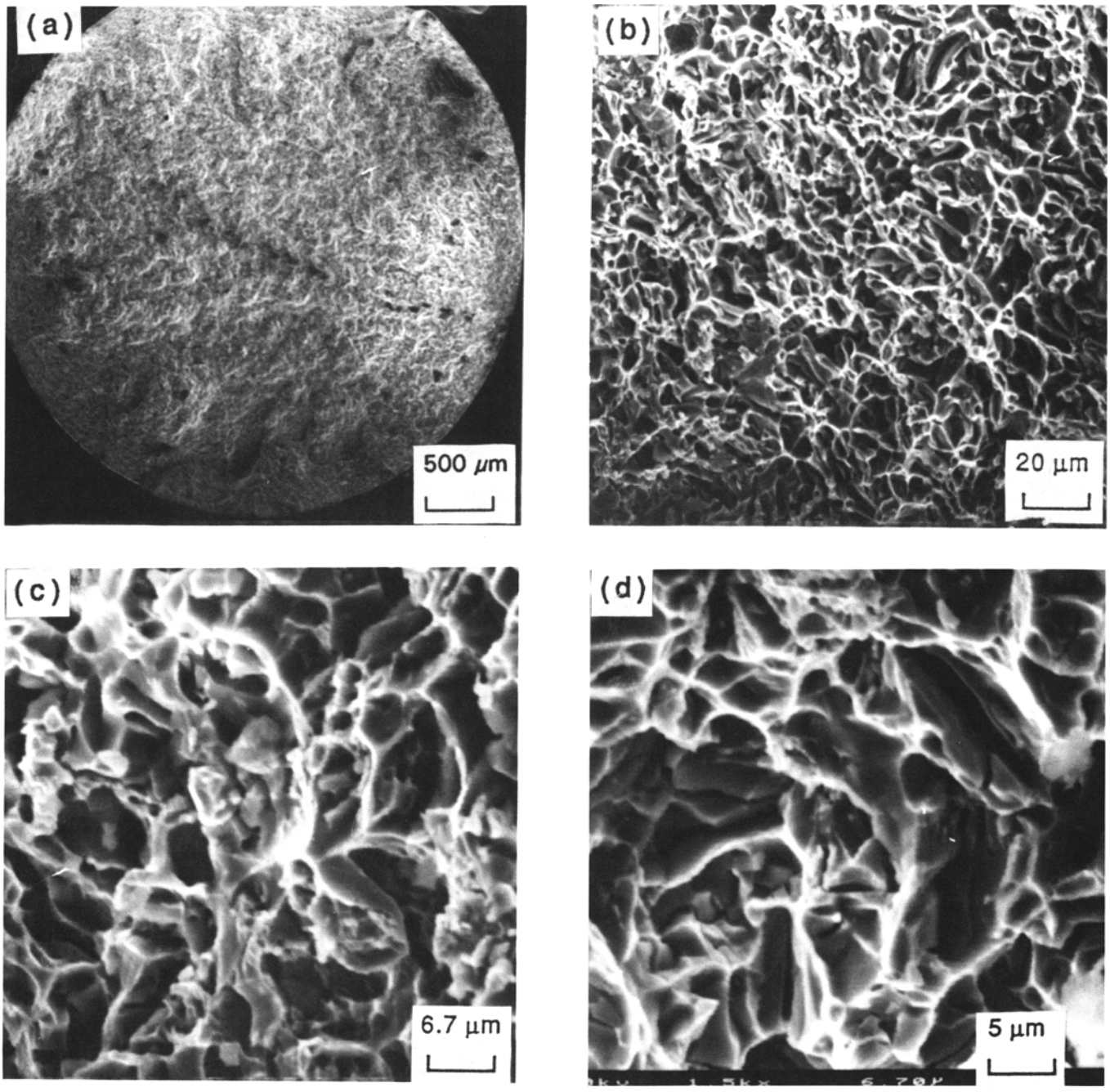

Fig. 7 Scanning electron micrographs of the high-cycle fatigue fracture surface of the I/M-processed (as-sand-cast) alloy (σ_{max} = 198 MPa, N_f = 444,578 cycles) showing (a) overall morphology showing random distribution of voids, (b) population of voids, (c) microscopic cracks, and (d) region of overload

ticles and numerous macroscopic voids, of varying size and shape, distributed uniformly through the fracture surface (Fig. 6a). High-magnification observations revealed fatigue fracture to be reminiscent of locally brittle mechanisms with the presence of numerous cracked particles of silicon (Fig. 6b). A careful examination of the stable crack growth and overload regions revealed the fine microscopic cracks to be localized at the coarse primary silicon through either cracked particulates or interfacial failure, or a combination of both (Fig. 6c). This provides evidence for the localization of plastic strain and the concomitant stress concentration. When the local stress concentration exceeds the strength of the silicon particle, failure of the particle through either cracking or decohesion at the interfaces is favored. This is exacerbated by the intrinsic brittleness of the primary silicon particulates.

The sample cyclically deformed at the lower stress of 198 MPa (N_f = 444,578 cycles) revealed distinct regions of crack initiation, stable crack growth, and overload (Fig. 7a). High-magnification observations in the region of stable crack growth revealed voids of a wide range of sizes (Fig. 7b), and numerous fine microscopic cracks (Fig. 7c). The overload region revealed numerous microscopic cracks, cracked particulates of

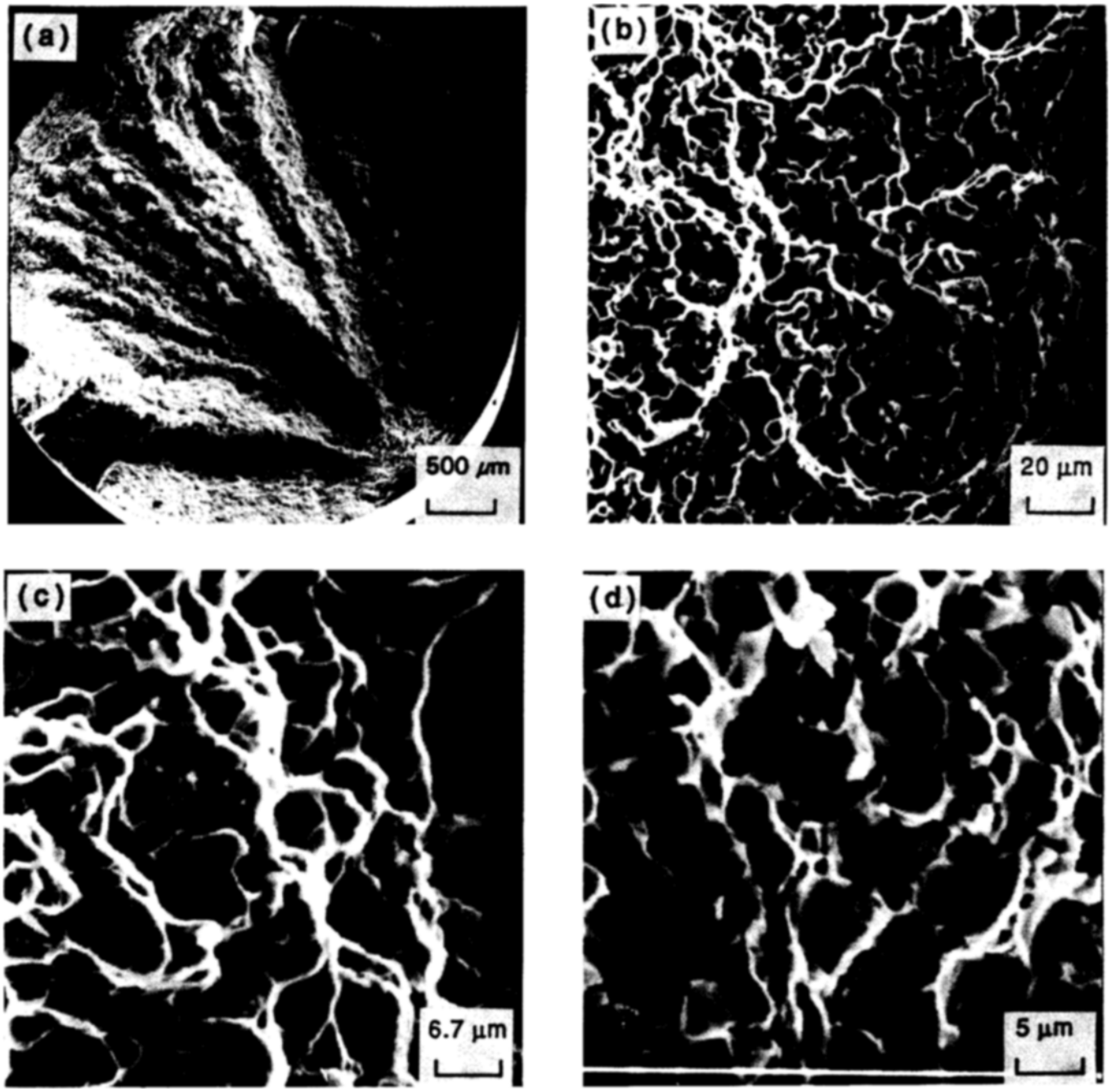

Fig. 8 Scanning electron micrographs of the high-cycle fatigue fracture surface of the spray deposition processed alloy (σ_{max} = 326 MPa, N_f = 35,392 cycles) showing (a) overall morphology, (b) population of voids and shallow dimples, (c) microscopic cracks, and (d) high magnification of (c)

coarse primary silicon, and isolated pockets of shallow dimples (Fig. 7d).

4.3.2 Spray Deposition Processed Alloy (AS17)

At high cyclic stress amplitude of 326 MPa and resultant cyclic fatigue life of 35,392 cycles, the fracture surface revealed a small yet distinct region of crack initiation and stable crack growth, and a large area of essentially overload failure (Fig. 8a). High-magnification observations in the region of stable crack growth revealed a near-uniform distribution of voids of varying size, isolated pockets of shallow near-equiaxed shaped dimples (Fig. 8b), and numerous fine microscopic cracks. The fine microscopic cracks were dispersed in the center of the dimples and along the grain boundaries (Fig. 8c). The average size of the dimple was larger than the average size of the coarse primary silicon particulates, indicative of the extensive plasticity-sustaining capability of this microstructure at the microscopic level.

At the lower cyclic stress amplitude of 257 MPa and resultant fatigue life of 386,272 cycles, overall fracture morphology revealed distinct regions of stable crack growth and overload (Fig. 9a). High-magnification observations in the region of sta-

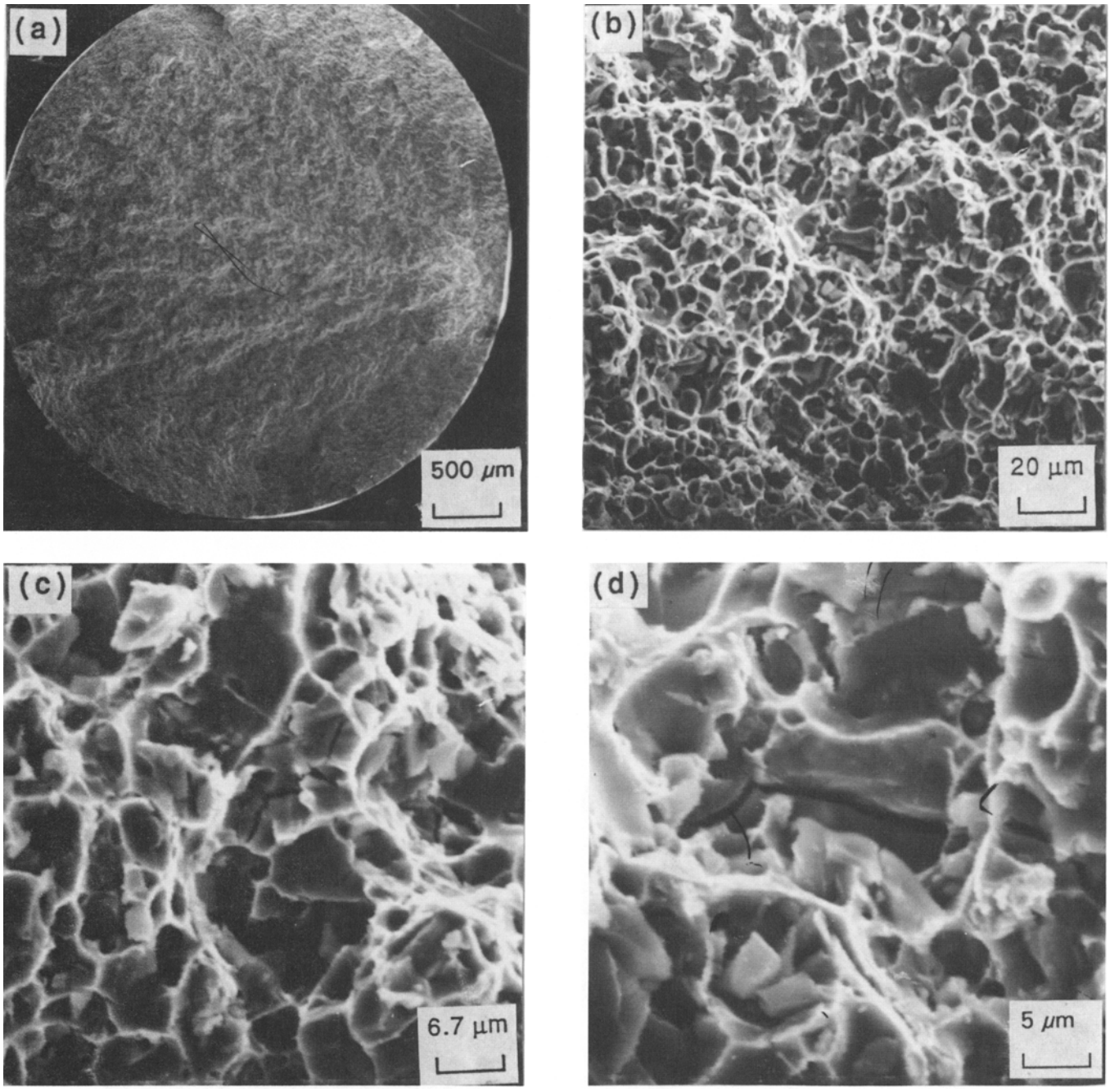

Fig. 9 Scanning electron micrographs of the high-cycle fatigue fracture surface of the spray deposition processed alloy (σ_{max} = 257 MPa, N_f = 386,272 cycles) showing (a) overall morphology, (b) population of voids and shallow dimples, (c) microscopic cracks, and (d) high magnification of (c)

ble crack growth revealed a uniform distribution of voids of varying size (Fig. 9b), isolated pockets of fine microscopic cracks (Fig. 9c), and shallow dimples, with microstructurally induced deflections of the crack as it traversed the alloy microstructure (Fig. 9d).

The overall macroscopically brittle and microscopically ductile failure mode accords well with that of aluminum alloy base matrices reinforced with fine ceramic particulates. The suppression of large areas of microcracking results in a higher energy absorbing ductile transgranular rupture. The overall number density and size of the dimples does reveal a significant difference in microplasticity between the spray atomized and deposition processed sample and the conventional I/M-processed (as-sand-cast) counterpart.

5. Conclusions

A study of the cyclic fatigue and fracture behavior of spray atomized and deposited hypereutectic aluminum-silicon alloy provides the following observations:

- Microstructure of a conventional I/M-processed alloy revealed coarse silicon particulates, of varying size, distributed randomly through the microstructure. At regular intervals the particulates revealed agglomeration. The spray deposition processed alloy revealed fine particulate-shaped silicon dispersoids distributed uniformly through the microstructure and equiaxed grains.
- The cycles to failure for fully reversed strain amplitude-controlled cycling is considered minimum for the alloy due to its limited cyclic plasticity at ambient temperature. The variation of maximum stress with fatigue life shows a trend expected of nonferrous metals. At equivalent values of maximum stress the spray atomized and deposition processed alloy reveals at least two to three orders improvement in high-cycle fatigue life over the conventional I/M-processed counterpart.
- High-cycle fatigue fracture of the conventionally as-sand-cast processed alloy (A390) was essentially brittle at both the macroscopic and microscopic levels, with numerous voids, cracked silicon particles, and decohesion at the particle-matrix interfaces. The spray deposition processed alloy (AS17) appeared brittle macroscopically, but revealed features microscopically reminiscent of locally ductile and brittle mechanisms. Suppression of microscopic cracking through cracking of the silicon particulates and decohesion at the interfaces resulted in distributed microplasticity in the fine microstructure and a resultant higher-energy-absorbing transgranular fracture mode. Shallow dimples were evident on the transgranular fracture surface with evidence of microstructurally induced deflections of the macroscopic cracks.

Acknowledgment

Dr. Y. Wu and Professor E.J. Lavernia gratefully acknowledge the financial support provided by the National Science Foundation (Grant No. DMI: 9528684) and the material support from Reynolds Metals Company (Richmond, VA). Mr. Anand acknowledges the University of Akron for research support (Grant No. 2-07699).

References

1. N. Kuroishi, Y. Odani, and Y. Takeda, *Met. Powder Rep.*, Vol 40, 1985, p 642-645
2. J. Zhou, J. Duszczyk, and B.M. Korevaar, *J. Mater. Sci.*, Vol 26, 1991, p 3041-3049
3. F. Yilmaz and R. Elliott, *J. Mater. Sci.*, Vol 24, 1989, p 2065-2070
4. I. Yamaguchi, I. Ohnaka, S. Kawamoto, and T. Fukusako, *Trans. Jpn. Inst. Met.*, Vol 27, 1986, p 195-203
5. J. Zhou and J. Duszczyk, *J. Mater. Sci.*, Vol 25, 1990, p 4541-4548
6. S. Anand, T.S. Srivatsan, Y. Wu, and E. J. Lavernia, *J. Mater. Sci.*, Vol 32, 1997 (in press)
7. M. Motomura, T. Haga, and Y. Sakurai, *J. Jpn. Inst. Light Met.*, Vol 38, 1988, p 528-533
8. J.L. Estrada and J. Duszczyk, *J. Mater. Sci.*, Vol, 25, 1990, p 1381-1391
9. A. Leatham, *Adv. Mater. Process.*, 8 Aug 1996, p 31-34
10. A.L. Moran and D.R. White, *J. Met.*, July 1990, p 21-24
11. D. Apelian, A. Lawley, G. Gillen, and P. Mathur, "Spray Deposition: A Fundamental Study of Atomization," Office of Naval Research, Arlington, VA, Technical Report, Sept 1985
12. D. Apelian, A. Lawley, G. Gillen, and P. Mathur, "Spray Deposition: A Fundamental Study of Droplet Impingement, Spreading and Consolidation," Office of Naval Research Technical Report, Sept 1996
13. M. Gupta, F.A. Mohamed, and E.J. Lavernia, *Metall. Trans., A*, Vol 23A, 1992, p 831-843
14. Y. Wu and E.J. Lavernia, *J. Met.*, Vol 43, No. 8, 1991, p 16-23
15. M. Gupta, F.A. Mohamed, and E.J. Lavernia, *Mat. Manuf. Process.*, Vol 5, No. 2, 1993, p 165-196
16. T.S. Srivatsan and E.J. Lavernia, *Processing and Fabrication of Advanced Materials for High Temperature Applications II*, V.A. Ravi and T.S. Srivatsan, Ed., The Minerals, Metals and Materials Society, 1992, p 141-169
17. S. Ping Yan, F.A. Mohamed, E.J. Lavernia, and T.S. Srivatsan, *J. Mater. Sci.*, Vol 30, 1995, p 4726-4736
18. Y. Wu, W.F. Cassada, and E.J. Lavernia, *Metall. Trans., A*, Vol 26A, 1995, p 1235-1245
19. E.J. Lavernia, *Int. J. Rapid Solidif.*, Vol 5, 1989, p 47-85
20. M. Gupta, F.A. Mohamed, and E.J. Lavernia, *Mater. Sci. Eng.*, Vol 144A, 1991, p 99-110
21. T.S. Srivatsan, T.S. Sudarshan, and E.J. Lavernia, *Prog. Mater. Sci.*, Vol 39 (No. 4/5), 1995, p 317-409
22. J. Zhang, M.N. Gungor, and E.J. Lavernia, *J. Mater. Sci.*, Vol 28, 1993, p 1515-1524
23. X. Liang, J. Earthman, and E.J. Lavernia, *Acta Metall.*, Vol 40, 1992, p 3303-3015
24. M. Gupta, T.S. Srivatsan, F.A. Mohamed, and E.J. Lavernia, *J. Mater. Sci.*, Vol 28, 1993, p 2245-2259
25. T.S. Srivatsan and E.J. Lavernia, *J. Mater. Sci.*, Vol 27, 1992, p 5965-5981
26. E.J. Lavernia, E. Gutierrez, J. Szakely, and N.J. Grant, *Prog. Powder Metall.*, Vol 43, 1987, p 683-709
27. S. Annavarapu, D. Apelian, and A. Lawley, *Metall. Trans., A*, Vol 19A, 1988, p 3077-3086